Physics and Chemistry of the Earth 36 (2011) 232–240

Contents lists available at ScienceDirect

Physics and Chemistry of the Earth

journal homepage: www.elsevier.com/locate/pce

Analysis of the relationship between flooding area and water height in the Logone floodplain

Hahn Chul Jung [a,b,*], Doug Alsdorf [a,b], Mark Moritz [c], Hyongki Lee [a], Sara Vassolo [d,e]

[a] School of Earth Sciences, The Ohio State University, Columbus, OH, USA
[b] Byrd Polar Research Center, The Ohio State University, Columbus, OH, USA
[c] Department of Anthropology, The Ohio State University, Columbus, OH, USA
[d] Bundesanstalt für Geowissenschaften und Rohstoffe (BGR), Stilleweg 2, D-30655, Hannover, Germany
[e] Lake Chad Basin Commission, (LCBC), Rond Point de L'Etoile, N'Djamena, Republic of Chad

ARTICLE INFO

Article history:
Received 14 October 2010
Received in revised form 21 December 2010
Accepted 20 January 2011
Available online 26 January 2011

Keywords:
Chad Basin
Flood
Landsat ETM+
Logone floodplain
Hydrology
Inundation

ABSTRACT

The intra- and inter-annual variations in the area, depth, and duration of seasonal flooding have direct and indirect impacts on ecosystems and human lives and livelihoods in the Logone floodplain, located in the Chad Basin. Flood inundation mapping helps us to better understand the variation in flooding and its impact on dynamic coupled human and natural systems in the Logone floodplain. We generated flood maps from 33 multi-temporal Landsat Enhanced Thematic Mapper Plus (ETM+) images acquired during three years from 2006 to 2008. Flooded area is classified using a short-wave infrared band whereas open water is classified by Iterative Self-organizing Data Analysis (ISODATA) clustering. The maximum flooding area in the Logone floodplain reached up to ~5.8 K km^2 in late October 2008. A second polynomial regression model showed a strong correlation between the flooding areas and water height variations in both the floodplain and the Logone River. The water heights stem from ENVISAT altimetry in the floodplain and gauge measurements in the river. Coefficients of determination between flooding areas and water height variations are greater than 0.91 with 4–36 days in time lag between the two measurements. Floodwater drains back to the river and to the northwest during the recession period in December and January. The study contributes to a better understanding of the Logone floodplain dynamics with details of the spatial pattern and size of the flooding area.

Published by Elsevier Ltd.

1. Introduction

The Logone floodplain in the Lake Chad Basin is an excellent example of coupled human and natural system (Liu et al., 2007). There are strong couplings between the hydrological, ecological and social systems as the area, depth, and duration of seasonal flooding have an impact on vegetation quality and quantity, fish and other animal populations as well as human livelihoods. The floodplain supports more than 20 million people as local communities use it for agriculture, fishing and dry season grazing (Scholte, 2005). The productivity and carrying capacity of the Logone floodplain is highly correlated with the area of the flooding (Loth, 2004). Wetland loss in the Logone floodplain has been accelerated due primarily to anthropogenic and natural processes, which impact the magnitude of flooding, and threatens the ecosystems. From 1988 to 2003, the Waza Logone Project of the International Union for Conservation of Nature (IUCN) has been instrumental in rehabilitating the degraded Logone floodplain. The general objective of the Waza Logone project was to achieve long-term enhancement of the biodiversity of the Logone area and to provide a sustainable improvement to the welfare of its rural population (Loth, 2004; Scholte, 2005). Climate variability and increased human water consumption have caused large changes in the water balance of the Lake Chad Basin. For example, the annual mean discharge of the Logone/Chari River system at N'Djamena has decreased by almost 75% over the last 40 years, from about 40 km^3/yr in the early 1960s to 10–15 km^3/yr in the 1980s and 1990s (Olivry et al., 1996; Coe and Foley, 2001).

Monitoring flood inundation areas of basins as well as water level changes of rivers and floodplains is necessary for understanding flood hazards, methane production, sediment transport, and nutrient exchange. The Logone floodplain includes flood-prone nations situated within this International River Basin (IRB), as the Logone River forms part of the international border between Chad and Cameroon. The challenge of issuing effective flood forecasts can be particularly difficult to overcome when there is no political agreement between riparian nations to share hydrologic information in real time for proactive flood management (Hossain and Katiyar, 2006). The member countries of the Lake Chad Basin

* Corresponding author. Address: NASA Goddard Space Flight Center, Code 614.3, Bldg 33, Rm G218, NASA GSFC, Greenbelt, MD 20771, USA. Tel.: +1 301 614 6839; fax: +1 614 292 4697.
E-mail address: jung.196@osu.edu (H.C. Jung).

1474-7065/$ - see front matter Published by Elsevier Ltd.
doi:10.1016/j.pce.2011.01.010

Commission (LCBC) have signed a data exchange protocol that covers this issue (LCBC, 2010). However, the wetlands of lowland rivers and lakes are massive in size and in volumetric fluxes, which greatly limits a thorough understanding of their flow dynamics. Most of the major river systems in the Sahel region of West Africa contain extensive floodplains. In an average year the total inundated area of the major floodplains in the Sahel is ~67 K km^2 (Loth, 2004). The Logone floodplain in northern Cameroon contains 10% of the total surface areas summed from major inland wetlands in the West African Sahel (Wesseling et al., 1994). Another difficulty when studying the floodplain is the complexity of flood dynamics. Water flow across wetlands is more complex than implied by point-based measurements. Flow paths and water sources are not fixed in space and time, but rather vary with floodwater elevations. Because of the size and complexity of the Logone floodplain dynamics, satellite remote sensing can play an important role in flood monitoring in the Logone floodplain.

The growing availability of satellite data has increased the opportunities to estimate water height variation and map flood inundation in floodplains from space (Smith, 1997; Alsdorf et al., 2007). Different remote sensing techniques and hydrological modeling approaches have been used to study the hydrology and floodplain dynamics in the Lake Chad Basin. First, TOPEX/POSEIDON radar altimetry was processed for measuring water surface elevations of rivers and wetlands (e.g. Birkett, 2000; Coe and Birkett, 2004; Crétaux and Birkett, 2006). Second, flooded areas and measure annual flooding areas have been identified using Landsat 1 (e.g. Benech et al., 1982), ENVISAT Advanced Synthetic Aperture Radar (ASAR) and SPOT optical image (e.g. Westra et al., 2005), and Moderate-Resolution Image Spectrometer (MODIS) (e.g. Westra and De Wulf, 2009). The third approach includes combining hydrological modeling with Shuttle Radar Topography Mission (SRTM) data to simulate the water balance of the basin (e.g. Coz et al., 2009) and developing a sophisticated hydrodynamic model with in situ measurements to assess the restoration potential of the Logone floodplain (e.g. Evans et al., 2003).

Here, we present a study of the relationship between flooding areas and water height variations in the Logone floodplain using space borne data. Flooding areas are calculated from the most recent data from the Landsat sensor Enhanced Thematic Mapper Plus (ETM+) whereas water height variations are provided from ENVISAT altimetry in the floodplain and gauge stations in the river. The results will significantly add to our understanding of the Logone floodplain dynamics and provide an opportunity to investigate the impacts of flood hazards in the highly interconnected ecological and social systems in the Logone floodplains.

2. Study area

The Logone floodplain, known locally as the *Yaayre*, is located in the Lake Chad Basin, Africa (Loth, 2004). The Lake Chad Basin is immense, covering an area of 2.5 M km^2 (Crétaux and Birkett, 2006; Coz et al., 2009) as compared with the Amazon Basin area of 6.0 M km^2 and the Congo Basin area of 3.5 M km^2. The Logone River is a major tributary of the Chari River. The Logone/Chari River waters flow into the Lake Chad Basin from the south and gradually move northwards, supplying permanent open water and seasonally inundating the marsh regions. Approximately 90% of the Lake Chad's water stems from the Logone/Chari River system. These rivers have their origins in Cameroon and the Central African Republic, respectively. The remaining 10% stems from other tributaries and local precipitation (FEWS, 1997).

The Logone floodplain lies south of Lake Chad and northeast of the Mandara Mountains (Fig. 1). The climate is semi-arid and the average annual rainfall varies from 750 mm/yr in the south to 550 mm/yr in the north (Westra and De Wulf, 2009). A Landsat ETM+frame, with a size of 176 × 171 km, includes the floodplain (Table 1). The superimposed SRTM elevation map in Fig. 1a shows that the study area is so flat as the topography slope is ~0.6 m/km. The basin topography apart from some local mountains is quite flat as indicated by the overall median slope value of ~1.3% south–north gradient (Coz et al., 2009). This flatness leads to the existence of extensive floodplains, which play a significant role in the regional water balance by redistributing water through evaporation (Gac, 1980; Olivry et al., 1996). The flooded area appears very dark green[1] in Fig. 1b. The inundation mechanism depends to a great degree on rainfall patterns. The first rains, which normally occur in May, saturate the soils and begin to fill the deepest depressions. Overbank flow is, however, by far the biggest contributor to the inundation of the floodplain, which takes place from September to October (MacDonald, 1993, 1999). The annual overbank flooding reduces both the peak flows and total volume of water in the Logone River. Water stored on the floodplain is returned during the recession period. The floodplain regulates the river by distributing flows throughout the year (Loth, 2004). Other factors affecting floodplain inundation is the Maga dam and the Logone River embankments. The Maga dam and an embankment along the left bank of the Logone River were built in 1979 to create a reservoir for a rice irrigation scheme and protect it from inundation (Loth, 2004).

3. Materials and methods

3.1. Landsat ETM+data

Landsat ETM+(i.e. Landsat 7) is the most recent in a series of Landsat sensors that have a 30 × 30 m spatial resolution and with a 16-day revisit capability to provide a balance between requirements for localized high spatial resolution studies and large area monitoring (Arvidson et al., 2001; Goward et al., 2001; Williams et al., 2006). Table 1 summarizes the Landsat ETM+dataset from 2006 to 2008 used in this study. The 33 scenes are available in the USGS Earth Resources Observation and Science Center (EROS) archive at no charge. All the acquisitions are processed to Standard Terrain Correction (Level 1T) for the research.

Two primary limitations to the utility of Landsat ETM+data are (1) the availability of cloud-free surface observations and (2) the failure of the Scan Line Corrector (SLC) that compensates for the forward motion of the satellite. Clouds are common features of visible and infrared remotely-sensed images collected from many tropical, humid, mountainous, and coastal regions of the world (Martinuzzi et al., 2007). Cloud cover reduces the number of Landsat surface observations. To construct a time series dataset at a finer temporal resolution, despite masking out cloud areas, Landsat ETM+data were collected with a cloud cover of less than 40% from USGS Global Visualization Viewer for the 3-year study period. Cloud and cloud-shadow were determined from the blue reflectance value. The cloud cover areas were derived from a majority analysis of 3 by 3 window size for pixels in which blue reflectance (i.e. Landsat ETM+band 1) is greater than 0.2. The cloud-shadow areas were then masked by the cloud areas including 10 pixel buffer zones (Sakamoto et al., 2007). A SLC instrument malfunction occurred onboard Landsat 7 on 31 May 2003 (NASA, 2009). The Landsat 7 ETM+is still capable of acquiring useful image data with the SLC turned off, reducing the usable data in each SLC-off scene by about 22% (Maxwell et al., 2007). The NASA gap filling software developed in IDL programming (Storey et al., 2005; NASA, 2009)

[1] For interpretation of color in Figs. 1, 2 and 5, the reader is referred to the web version of this article.

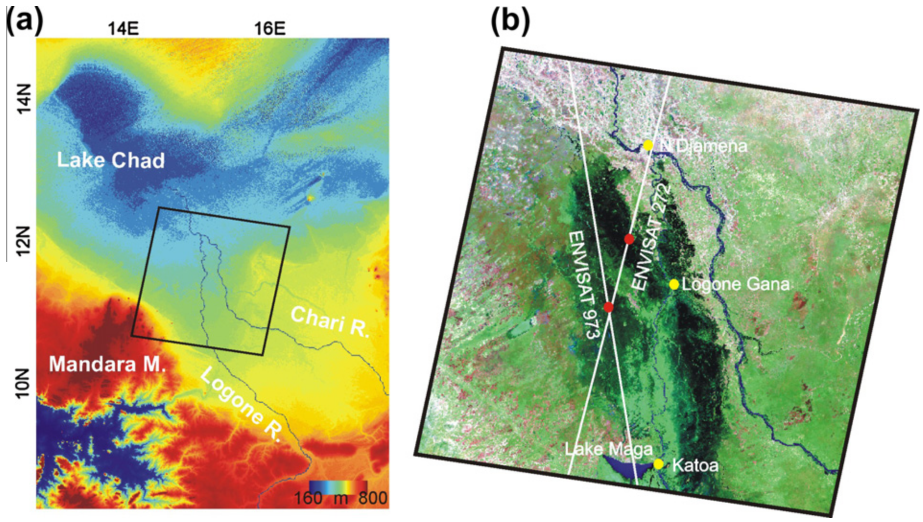

Fig. 1. (a) SRTM elevation map of the Lake Chad Basin. Logone floodplain at the south of the Lake Chad is hydrologically linked with two major branches of the Logone and Chari Rivers. Black diagonal box indicates Landsat ETM+frame used for flood inundation mapping. (b) Landsat ETM+color composite (R: band 7, G: band 4, B: band 2) in the Logone floodplain. ENVISAT altimetry ground tracks (i.e. ascending pass 973 and descending pass 272) and measurements are marked with white lines and red dots. Local river gauge stations are marked with yellow dots. (For interpretation of the references to colour in this figure legend, the reader is referred to the web version of this article.)

Table 1
Summary of Landsat ETM+dataset and classification results.

Site location (path/row)	Acquisition date	Flooded (km^2/%)[a]	Nonflooded (km^2/%)	Cloud/cloud-shadow (km^2/%)
Logone floodplain (P184/R052)	4 January 2006	678/2	29,175/98	0/0
	5 February 2006	211/1	29,000/97	642/2
	25 March 2006	34/0	29,819 /100	0/0
	10 April 2006	15/0	28,360/95	1478/5
	26 April 2006	65/0	24,984/84	4805/16
	28 May 2006	77/0	29,777/100	0/0
	15 July 2006	129/0	28,238/95	1487/5
	1 September 2006	526/2	28,997/97	330/1
	17 September 2006	1199/4	28,165/94	489/2
	3 October 2006	2702/9	23,557/79	3594/12
	20 November 2006	3958/13	25,896/87	0/0
	6 December 2006	2847/10	27,006/90	0/0
	22 December 2006	1385/5	28,469/95	0/0
	7 January 2007	453/2	29,401/98	0/0
	8 February 2007	100/0	29,753/100	0/0
	24 February 2007	1/0	29,745/100	108/0
	12 March 2007	17/0	29,837/100	0/0
	28 March 2007	15/0	29,152/98	687/2
	13 April 2007	18/0	22,119/74	7716/26
	31 May 2007	49/0	29,379/98	425/1
	23 November 2007	2731/9	27,123/91	0/0
	9 December 2007	1663/6	28,191/94	0/0
	25 December 2007	843/3	29,010/97	0/0
	26 January 2008	253/1	29,601/99	0/0
	11 February 2008	158/1	29,695/99	0/0
	27 February 2008	89/0	29,765/100	0/0
	14 March 2008	17/0	29,178/98	658/2
	30 March 2008	60/0	29,793 /100	0/0
	15 April 2008	32/0	29,821/100	0/0
	18 June 2008	43/0	23,228/78	6583/22
	24 October 2008	5764/19	24,089/81	0/0
	9 November 2008	4894/16	23,538/79	1422/5
	25 November 2008	5014/17	24,840/83	0/0

[a] Flooded class excludes open water of Logone/Chari Rivers and Lake Maga with an area of ~279 km^2 in the Landsat ETM+swath.

goes through two steps to fill gaps in the Landsat ETM+dataset used in the study. The first step, re-framing, processes all of the input imagery to create images that have the same dimensions in line length and number of lines. The second step replaces the no-data pixels in the image by linear least squares regression analysis using their counterparts in temporally close and in anniversary scenes.

The short-wave infrared (SWIR) data was used to identify flooded area in the study area. SWIR data are highly sensitive to moisture content in the soil and the vegetation canopy (Sakamoto et al., 2007). Westra and De Wulf (2009) have recently demonstrated that the Moderate-Resolution Imaging Spectroradiometer (MODIS) band 7 (wavelength: 2.105–2.155 μm) provides better results for delineating the flooding area in the Logone floodplain rather than the MODIS Normalized Difference Vegetation Index (NDVI) and the MODIS Normalized Difference Water Index (NDWI). A threshold of 0.08 in reflectance unit was used to calculate the flooding area for the 2000–2005 periods. The threshold was tested and proven based on cumulative runoff in the catchment area and estimation of the soil moisture prior to the flooding (Westra and De Wulf, 2009). To apply the approach to all of the acquired Landsat ETM+data used in the study, the digital numbers (DN) of the original Landsat ETM+band 7 (wavelength: 2.09–2.35 μm) were converted through spectral radiance at the sensor's aperture into top of atmosphere (TOA) reflectance. The detail of the conversion follows equations described in the Landsat 7 science data user's handbook (NASA, 2009). The converted planetary TOA reflectance incorporates the solar zenith angle, earth–sun distance, and calibrated radiance related to outer space radiance, thus considering the conversion from DN to reflectance unit as requiring correction for quantitative remote sensing applications (Liang et al., 2002; Ouaidrari and Vermote, 1999). Open water of the Logone/Chari Rivers and of Lake Maga was classified from a Landsat 7 SLC-on image dated 21 October 2001. The water bodies mask out the classified flooded/nonflooded areas to focus on floodplain inundation dynamics for the 3-year study period. The Iterative Self-organizing Data Analysis (ISODATA) clustering method was implemented to classify the open water. ISODATA is an unsupervised classification scheme that uses an iterative approach incorporating a number of heuristic procedures to compute classes (Tou and Gonzales, 1974; Melesse and Jordan, 2002). The ISODATA utility in the study repeats the clustering of the image into 20 classes until the number of pixels in a class reaches twice a threshold of 0.05% for the minimum number of pixels in two successive iterations of the clustering.

3.2. ENVISAT altimetry data

The ENVISAT altimeter data were selected and processed from January 2006 to December 2008. The ENVISAT orbits on a 35-day repeat cycle with 98.5° inclination. The ENVISAT Geophysical Data Record (GDR) contains 18-Hz retracked measurements, corresponding to an along-track ground spacing of approximately 350 m. In this study, ICE-1, which has been proved to perform well over inland water bodies (Frappart et al., 2006a; Lee et al., 2010), retracked measurements are used. The instrument corrections, media corrections (i.e. dry troposphere correction, wet troposphere correction calculated by the French Meteorological Office (FMO) from the European Centre for Medium-Range Weather Forecasts (ECMWF) model, and the ionosphere correction based on Global Ionosphere Maps (GIM)), and geophysical corrections (i.e. solid Earth tide and pole tide) have been applied. To identify the radar returns from the water surface, the 18-Hz ICE-1 backscattering coefficients are examined over the 18-Hz locations selected (Lee et al., 2009). The backscattered energy is generally higher over the floodplain than the surrounding dry land with moderate vegetation cover. We select the 18-Hz radar returns that have the backscattering coefficient higher than 20 dB, and spatially average them (i.e. red dots in Fig. 1b) to construct a time series in the Logone floodplain on ascending pass 973 and descending pass 272 (Fig. 3). The mean RMSEs of ENVISAT 973 and ENVISAT 272 altimetric measurements are 7 and 3 cm, respectively (see error bars of altimetric measurements in Fig. 3).

3.3. Ground-based data

In situ measurements of daily gauge height at Katoa, Logone Gana, and N'Djamena in the Logone River (see Fig. 1b) were used to compare with the Landsat-derived flooding areas and the ENVISAT radar altimetric water height variations. Missing data at Katoa and N'Djamena are filled with the average daily values for the previous years from 2000 to 2005. N'Djamena, Chad's capital city, is at the location where the Logone River empties into the Chari River. Logone Gana is located at the middle of the study area and Katoa lies at the east of Lake Maga to provide a time series of water heights in the Logone River.

4. Results and discussion

4.1. Flooding area

Flood inundation maps were generated from 33 Landsat ETM+scenes summarized in Table 1 (Fig. 2). The time interval between the successive flood maps varies from 16 days in the satellite

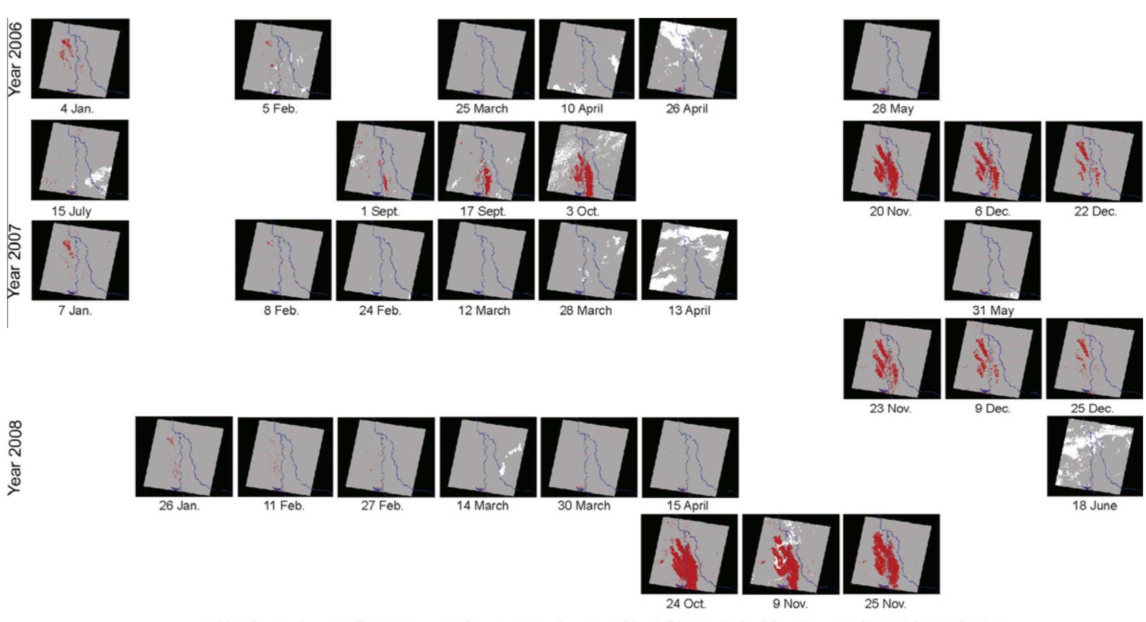

Fig. 2. Flood inundation maps derived from multi-temporal Landsat ETM+imagery. These are aligned with 16-day of the satellite repeat cycle with missing images in the time series. See text for processing details.

repeat cycle to 176 days from June to October 2007 during low water. Flooded area is classified and colored red in Fig. 2. The flooding inundates a large area of the Logone floodplain between Katoa and N'Djamena. Variability in flooding areas during high water are comparatively greater than during low water, thus illustrating yearly flooding in the study area. The flooding areas are less changeable during low water. The duration of the floodwater is generally 5 months from September to January. The finding supports that the saturated soils during rainy season (i.e. June–August) have no more capability for storing water and allow inundation of the floodplain for three to five months after the overbank flooding from the Logone River (Westra and De Wulf, 2009). The largest flooding area for the study period reaches ∼5.8 K km^2 and occupies ∼19% in the image on 24 October 2008 (Table 1). Despite excluding ∼1.3 K km^2 potential floodplain at the south of Lake Maga out of the used Landsat ETM+swath, the result is consistent with 6.7 ± 1.8 K km^2 in the mean MODIS-observed maximum flooding area from 2000 to 2005 (Westra and De Wulf, 2009). The maximum annual flooding areas of ∼4.0 K km^2 on 20 November 2006 and ∼2.7 K km^2 on 23 November 2007 are much less than that of 2008 because Landsat ETM+dataset in 2006 and 2007 do not include the maximum flooding period from late October to early November. Besides the sampling issue, the maximum area of the flooding varies highly from one year to another depending on the yearly amount of runoff and the soil moisture of the floodplain prior to flooding (Loth, 2004).

Cloud/cloud-shadow occupies up to 26% of the image on 13 April 2007. All of the images acquired during high water have less than 5% cloud/cloud-shadow covered except an image on 3 October 2006. A time series of flooding areas in the uppermost of Fig. 3 shows a smooth trend of the flooding area variation despite the cloud contamination. It suggests that most of the cloud/cloud-shadow areas are most likely nonflooded. But, flooding area seems to be underestimated by about 5% (i.e. ∼1.4 K km^2 cloud/cloud-shadow coverage on 9 November 2008), thus having a lower size of flooding area rather than both prior and posterior flood maps on 24 October and 25 November 2008 (see the last three bar graphs in Fig. 3).

4.2. Water height variation

Time series of water height variations are generated using ENVISAT altimetry in the floodplain and in situ measurements in the river (Fig. 3). The altimeter-observed height is relative to the reference ellipsoid whereas the river gauge height is with respect to a local datum. To compare relative water height variations from both the altimetry and the river gauges, they are converted into water heights above observed minimum in Fig. 3. ENVISAT altimetry provides 35-day repeated water height measurements in the floodplains (see ENVISAT pass 973 and ENVISAT pass 272 shown in Fig. 1b). The ENVISAT altimetric measurements were linearly interpolated to estimate daily water height variations between two successive altimetric measurements marked with circles in Fig. 3. The amplitude of water heights in ENVISAT pass 272 is ∼2.5 m, which is greater than the ∼1 m amplitudes observed in ENVISAT pass 973. Since ENVISAT pass 272 is in the proximity of the Logone River, it is more influenced by the overbank flooding from the river. The observed minimum altimetric ellipsoidal heights are 316.41 m in ENVISAT pass 973 and 307.79 in ENVISAT pass 272. The height difference can be indicative of the local slope in the floodplain, thus suggesting that floodwaters in ENVISAT pass 973 flow downhill to the north. Three local river gauge stations provide daily water heights at Katoa, Logone Gana, and N'Djamena. The river water amplitudes become greater downstream, compared to upstream, and they are all greater than those of altimetric measurements in the floodplain. The river water amplitudes are ∼3.5 m at Katoa, ∼5.5 m at Logone Gana, and ∼5.8 m at N'Djamena. The results are consistent with seasonal water height amplitudes of 5–6 m for the most southerly zones of the Logone and Chari Rivers and of 1–2 m for the wetland areas using TOPEX/POSEIDON altimetry from 1993 to 1998 (Birkett, 2000). Although Logone Gana and N'Djamena show similar amplitudes of the water height variations, the N'Djamena hydrograph becomes sharply increased and decreased more than Logone Gana. N'Djamena is located immediately after the confluence between Logone and Chari Rivers, thus the N'Djamena heights are a summation of the flows in these two rivers. The peak-level at Katoa is observed in late September, which is earlier than the late October peak-level periods at Logone Gana and N'Djamena. Birkett (2000) showed the phase lag of one to two months in water heights between the upstream Chari River and Lake Chad during the 1990s.

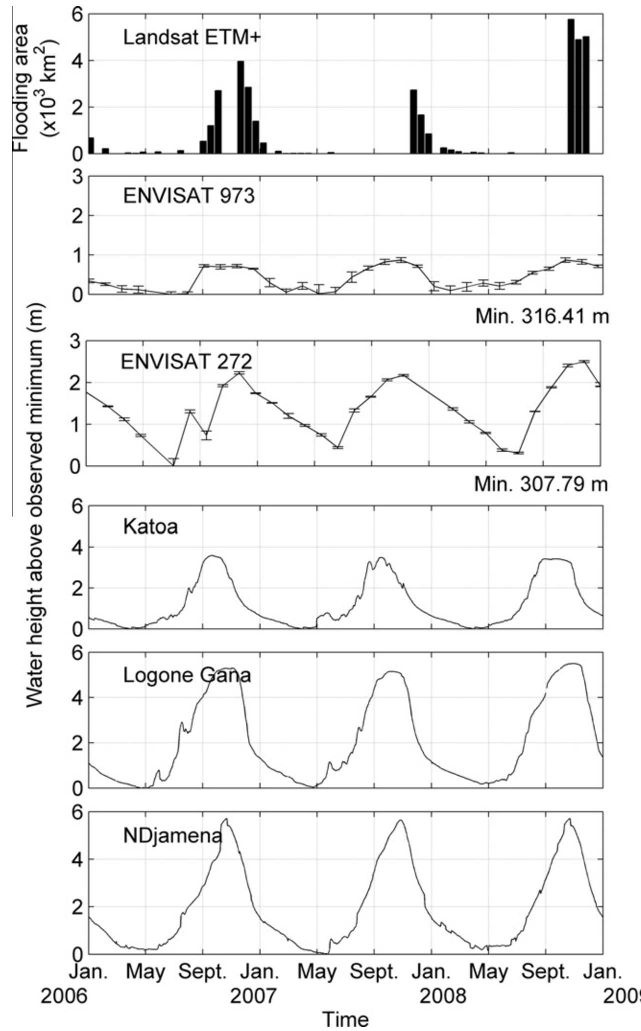

Fig. 3. Time series of flooding areas and water heights in the study area. Bar graphs in the uppermost panel represent flooding areas calculated from Landsat ETM+in Fig. 2. The ENVISAT altimetry provides 35-day repeated measurements of water height variation in the second and third upper graphs. These altimetric measurements are linearly interpolated between two successive points. Three local river gauge stations provide daily measurements at the bottom three graphs.

4.3. Correlation between flooding area and water height variation

A positive relationship with a time lag is found between flooding areas and water height variations for all five sites (Fig. 4). The correlations were calculated based on a second order polynomial regression model and time shifting. On the graphs, the *y*-axis represents flooding area and the x-axis represents the water height proportion of maximum height above observed minimum at each site. Coefficients of determination (i.e. R^2) range from 0.50 to 0.89 before time shifting. Altimetric water heights are more highly correlated with flooding areas than river gauge heights. The altimetric measurements are collected in the floodplain and they do not anticipate a large time lag between their water height variations and flooding areas as much as river gauge heights. After performing the optimized time shifting to best-fit the regression model, the correlations at river gauges increased to greater than 0.95. The delayed time shifting (i.e. phase lag) increases downstream compared to upstream. River gauge data at Katoa, Logone Gana, and N'Djamena have the highest correlations as they are shifted +36, +22, and +13 days, respectively. The correlations of the altimetric measurements also increase as they are shifted +4 and −15 days within the ENVISAT repeat cycle of 35 days. The time difference between flooding area and water height in altimetric measurements is caused by daily linear interpolation problem and internal ENVISAT altimetric measurement error.

The regression model calculates flooding areas only when water heights are above a threshold level of flooding. The model assumes no flooding event in the study area when water heights are less

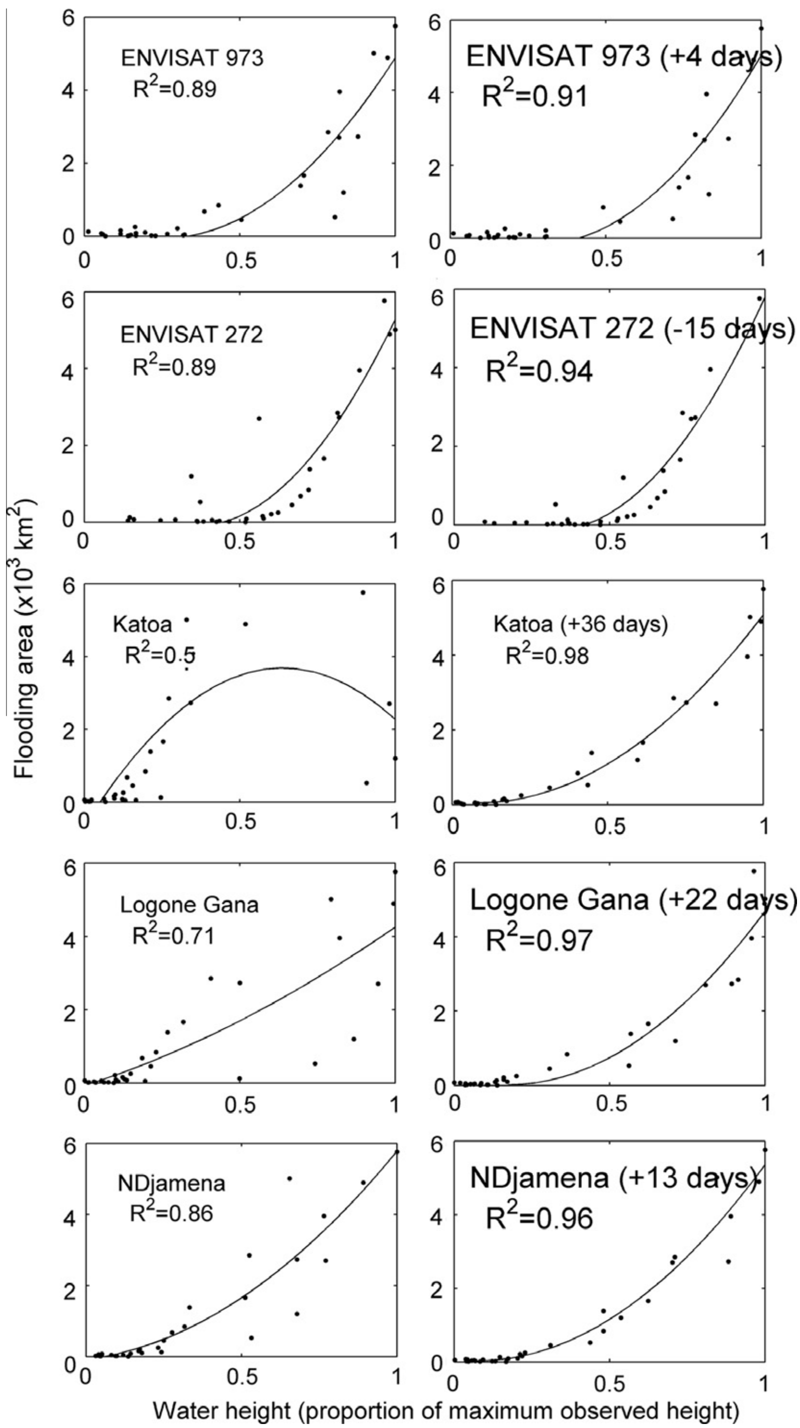

Fig. 4. Relationships of Landsat-derived flooding areas with water height variations from ENVISAT altimetry and river gauge stations. A second order polynomial regression and time shifting are performed to find the best-fit lines to a set of data points. Left/right graphs are the regression model results before/after time shifting. An increase in R^2 after time shifting represents phase lag between flooding areas and water height variations.

Table 2
Summary statistics for regression models in Fig. 4.

Site (±time shifting)	Regression model ($y = a \cdot x^2 + b \cdot x + c$; y: flooding area x: water height, a, b, c: constants)	R^2	x-intercept		
			H1 (prop.)[a]	H2 (cm)[b]	Q (m^3/s)[c]
ENVISAT 973	$8867 \cdot x^2 - 4493 \cdot x + 507$	0.89	0.34	31,670	
ENVISAT 973 (+4 days)	$10{,}169 \cdot x^2 - 5800 \cdot x + 650$	0.91	0.42	31,677	
ENVISAT 272	$13{,}110 \cdot x^2 - 9436 \cdot x + 1598$	0.89	0.45	30,891	
ENVISAT 272 (−15 days)	$12{,}651 \cdot x^2 - 7972\ x + 1112$	0.94	0.42	30,884	
Katoa	$-10{,}710 \cdot x^2 + 13{,}650 \cdot x - 666$	0.50	0.05	78	30
Katoa (+36 days)	$5976 \cdot x^2 - 998 \cdot x + 89$	0.98	0.08	88	43
Logone Gana	$1576 \cdot x^2 + 2753 \cdot x - 80$	0.71	0.03	21	13
Logone Gana (+22 days)	$6832 \cdot x^2 - 2372 \cdot x + 222$	0.97	0.17	100	116
N'Djamena	$4767 \cdot x^2 + 1089 \cdot x - 81$	0.86	0.06	89	81
N'Djamena (+13 days)	$6217 \cdot x^2 - 930 \cdot x + 65$	0.96	0.07	98	98

[a] H1 corresponds x-intercept in Fig. 4.
[b] H2 is the corresponding absolute water height to H1 with respect to the reference ellipsoid for ENVISAT altimetry and local datum for river gauge.
[c] Q is the corresponding flow rate to H2 based on local discharge rating curve from river gauge height.

Table 3
The estimation of flow rates for flooding areas in the regression models with time shifting.

Flooding area (km^2)	Flow rate (m^3/s)		
	Katoa	Logone Gana	N'Djamena
1000	374	386	835
2000	569	532	1280
3000	765	664	1660
4000	949	793	2010

than an x-intercept defined by the second order polynomial in Table 2. The water heights in x-intercepts at river stations are converted into flow rates based on local discharge rating curves from their absolute river gauge heights. The flow rate could be a good index of flooding intensity as floodwaters approach overbank flooding levels defined as H2 in Table 2. The regression model during high water on the x-axis becomes more sensitive to flooding areas on the y-axis due to lower degree of the freedom (i.e. more severe slope of the second polynomial fitting line) as compared to during low water. Table 3 summaries the corresponding flow rates to flooding areas during high water in the regression models with time shifting. The result suggests that flooding to 4000 km^2 in the study area is most likely to occur 36, 22, and 13 days after the flow rates exceed 949 m^3/s at Katoa, 793 m^3/s at Logone Gana, or 2010 m^3/s at N'Djamena, respectively.

4.4. Logone floodplain dynamics

The Logone floodplain dynamics are analyzed with monthly average flood probability maps (Fig. 5). The flood probability is calculated on a pixel-by-pixel basis from flood maps in the same month for the 3-year study period. The probability varies from 100% in flooded (i.e. red) into 0% in nonflooded (i.e. white). Blue represents open water such as Logone/Chari Rivers and Lake Maga. For instance, red areas on November map in Fig. 5 represent 100% flooding in all November flood maps (i.e. 20 November 2006, 23 November 2007, 9 November 2008, and 25 November 2008) whereas orange areas represent 50% flooding. The flood probabilities multiplied by a single pixel area of 900 m^2 are summed to calculate monthly average flooding areas. The monthly average

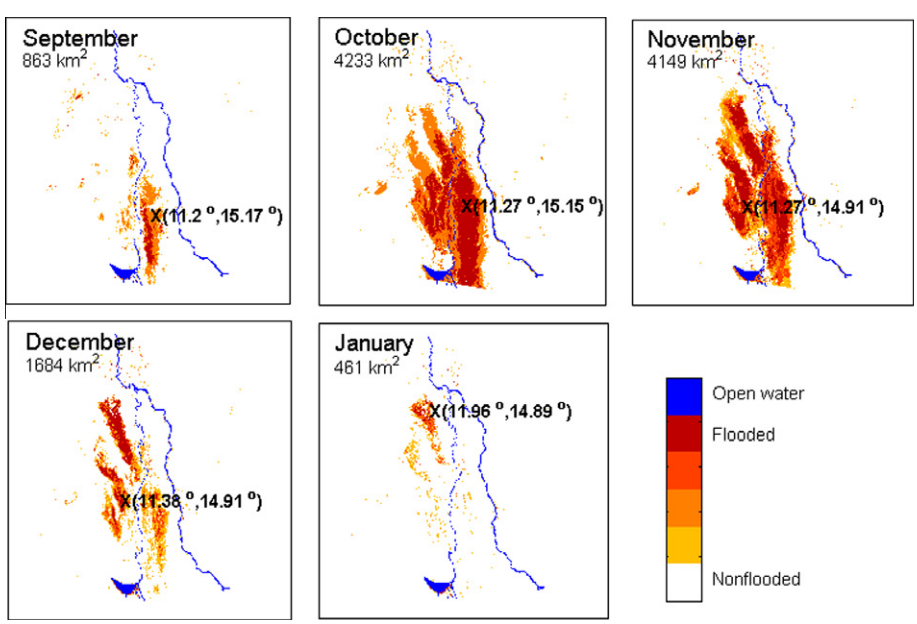

Fig. 5. The detailed spatial pattern and size of the flooding areas in the Logone floodplain during high water. Monthly average flooding areas are calculated based on monthly flood probability maps for the 3-year study period. As red goes gradually through orange to white, it ranges from 100% to 0% in the flood probability. Blue represents open water such as Logone/Chari Rivers and Lake Maga. The mode of the flooded area at each map is marked with "X" in latitude and longitude. (For interpretation of the references to colour in this figure legend, the reader is referred to the web version of this article.)

flooding area takes up 863 km^2 in September, reaches up to 4233 km^2 in October and 4149 km^2 in November during maximum flooding period, and reduces into 1684 km^2 in December and 863 km^2 in January during the drainage period.

The Logone floodplain clearly shows the spatial variation of flooding as well as the size of flooding area from September to January. Fig. 5 marks the most frequently flooded location (i.e. the mode in statistics) in latitude and longitude with "X" at each map. The monthly mode locations suggest that floodwater drains to the northwest and eventually into Lake Chad. In September, most flooded areas are located at the east side of the Logone River. In October and November, the flooded areas are spread out to both sides of the river, but the mode locations move from the east to the west. In December and January, the mode locations move rapidly toward the north with decreasing size of the flooding area.

The north of Lake Maga is mostly nonflooded even during the maximum flooding months of October and November in Fig. 5. This is consistent with the finding that the embankment along the Logone River protects the irrigated rice fields and that the Maga dam eliminates flooding, which results in a decrease of depth and area of the flooding because the dam intercepts discharge from the Logone River and the runoff from the Mandara Mountains (Loth, 2004).

5. Conclusions

This study shows a strong correlation between flooding areas and water height variations in the Logone floodplain using space borne data. The regression model can facilitate a flood monitoring system and can support a flood prediction system with a few weeks prior to the overbank flooding from the Logone River and in combination with river gauge data.

The multi-temporal Landsat ETM+imagery renders the first time series of flooding areas in the Logone floodplain for the recent three years. The high-resolution flood inundation maps provide a better understanding of the complex floodplain dynamics despite cloud/cloud-shadow contamination. The overbank flooding starts at the east of the Logone River in September. The monthly average flooding area increases to $\sim$4.2 K km^2 in October and November. As inflow reduces, the floodwater drains to the northwest in December and January. Loth (2004) pointed out that part of it returns back to the Logone River, part of it contributes to the groundwater through infiltration, and part of it is lost through evapotranspiration during recession period. The results confirm the claims of the local people that Maga dam and embankment influence the tributary network and discharge in the Logone floodplain to date since the construction in 1979.

Rainfall, runoff, soil moisture, and evapotranspiration by plants are not explored in parallel with water height variation to study the relationship with the degree of inundation in this study. These are less likely to influence the flooding system in the Logone floodplain, but the data deficiencies could explain some errors in the regression analysis. Another weakness of the study is that a time series of flooding areas has no flood map in August for the 3-year study period due to the unavailability of Landsat images.

Volumetric storage change can be estimated by combining flooding area with water height change. But, the depth of floodwaters varies too much in space and time in the floodplain thus the associated uncertainty and error assessment need to be considered (Frappart et al., 2006b). For a promising future research, having more dense water height measurements in the floodplain makes it feasible to estimate the storage change in the catchment.

Acknowledgements

This work was supported by NASA Headquarters under the NASA Earth and Space Science Fellowship Program (09-Earth09F-197). Funding for this research was also provided by a Korean Science and Engineering Foundation Grant (No. C00131) and by OSU's Climate, Water, and Carbon program. USGS EROS supplied the Landsat ETM+ data. ENVISAT radar altimetry data were provided by ESA/ESRIN. The river gauge data are courtesy of the Lake Chad Basin Commission.

References

Alsdorf, D.E., Rodriguez, E., Lettenmaier, D.P., 2007. Measuring surface water from space. Reviews of Geophysics 45, 1–24.

Arvidson, T., Gasch, J., Goward, S.N., 2001. Landsat 7′s long-term acquisition plan – an innovative approach to building a global imagery archive. Remote Sensing of Environment 78, 13–26.

Benech, V., Quensiere, J., Vidy, G., 1982. Hydrologie et physico-chimie des eaux de la plaine d'inondation du Nord Cameroun. Cahiers ORSTOM Series Hydrologique XIX (1), 15–35.

Birkett, C.M., 2000. Synergistic remote sensing of Lake Chad: variability of basin inundation. Remote Sensing of Environment 72, 218–236.

Coe, M.T., Birkett, C.M., 2004. Calculation of river discharge and prediction of lake height from satellite radar altimetry: example for the Lake Chad Basin. Water Resources Research 40. doi:10.1029/2003WR002543.

Coe, M.T., Foley, J.A., 2001. Human and natural impacts on the water resources of the Lake Chad basin. Journal of Geophysical Research 106, 3349–3356.

Coz, M.L., Delclaux, F., Genthon, P., Favreau, G., 2009. Assessment of Digital Elevation Model (DEM) aggregation methods for hydrological modeling: Lake Chad Basin, Africa. Computers & Geosciences 35, 1661–1670.

Crétaux, J.F., Birkett, C., 2006. Lake studies from satellite radar altimetry. Comptes Rendus Geosciences 338, 1098–1112.

Evans, S.Y., Bradbrook, K., Braund, R., Bergkam, G., 2003. Assessment of the restoration potential of the Logone floodplain (Cameroon). Water and Environment Journal 17, 123–128.

FEWS, 1997. Lake Chad untapped potential, famine early warning system. Special Report 97-4.

Frappart, F., Calmant, S., Cauhopé, M., Seyler, F., Cazanave, A., 2006a. Preliminary results of ENVISAT RA-2-derived water levels validation over the Amazon basin. Remote Sensing Environment 100, 252–264.

Frappart, F., Do Minh, K., L'Hermitte, J., Cazenave, A., Ramillien, G., Le Toan, T., Mognard-Campbell, N., 2006b. Water volume change in the lower Mekong from satellite altimetry and imagery data. Geophysical Journal International 167, 570–584.

Gac, J.Y., 1980. Géochimie du bassin du Lac Tchad (Geochemistry of Lake Chad basin). Thèse de Doctorat d'Etat, Travaux et Documents de l'ORSTOM, ORSTOM (Office de la Recherche Scientifique et Technique d'Outre-Mer). Paris, p. 252.

Goward, S.N., Masek, J.G., Williams, D.L., Irons, J.R., Thompson, R.J., 2001. The Landsat 7 mission, terrestrial research and applications for the 21st century. Remote Sensing of Environment 78, 3–12.

Hossain, F., Katiyar, N., 2006. Improving flood forecasting in international river basins. EOS Transactions American Geophysical Union 87, 49–60.

LCBC, 2010. Lake Chad Basin project. <http://lakechad.iwlearn.org/> (accessed 10.10).

Lee, H., Durand, M., Jung, H.C., Alsdorf, D., Shum, C., Sheng, Y., 2010. Characterization of surface water storage change in Arctic lakes using simulated SWOT measurements. International Journal of Remote Sensing 31, 3931–3953.

Lee, H., Shum, C., Yi, Y., Ibaraki, M., Kim, J.-W., Braun, A., Kuo, C.-Y., Lu, Z., 2009. Louisiana wetland water level monitoring using retracked TOPEX/POSEIDON altimetry. Marine Geodesy 32, 284–302.

Liang, S., Fang, H., Morisette, J.T., Chen, M., Shuey, C.J., Walthall, C.L., 2002. Atmospheric correction of Landsat ETM+land surface imagery: II. Validation and applications. IEEE Transactions on Geoscience and Remote Sensing 40, 2736–2746.

Liu, J., Dietz, T., Carpenter, S.R., Alberti, M., Folke, C., Moran, E., Pell, A.N., Deadman, P., Kratz, T., Lubchenco, J., Ostrom, E., Ouyang, Z., Provencher, W., Redman, C.L., Schneider, S.H., Taylor, W.W., 2007. Complexity of coupled human and natural systems. Sciences 317, 1513–1516.

Loth, P., 2004. The Return of the Water: Restoring the Waza Logone Floodplain in Cameroon. IUCN, Gland, Switzerland and Cambridge, UK.

Martinuzzi, S., Gould, W.A., González, O.M.R., 2007. Creating Cloud-free Landsat ETM+Data Sets in Tropical Landscapes: Cloud and Cloud-shadow Removal. USDA General Technical Report IITF-GTR-32.

Maxwell, S.K., Schmidt, G.L., Storey, J.C., 2007. A multi-scale segmentation approach to filling gaps in Landsat ETM+SLC-off images. International Journal of Remote Sensing 28, 5339–5356.

Melesse, A., Jordan, J.D., 2002. A comparison of fuzzy vs. augmented-ISODATA classification algorithms for cloud-shadow discrimination from Landsat images. Photogrammetric Engineering and Remote Sensing 68, 905–911.

MacDonald, Mott, 1999. Logone Floodplain Model Study Report. Mott MacDonald, Cambridge. UK.

MacDonald, Mott, 1993. Mathematic Model of the Hydrological Behaviour of Lake Chad and its Feeder Rivers. Mott MacDonald, Cambridge. UK.

NASA, 2009. Landsat 7 science data users handbook, Chapter 11-Data products. <http://landsathandbook.gsfc.nasa.gov/handbook/handbook_htmls/chapter11/chapter11.html>.

Olivry, J.C., Chouret, A., Vuillaume, G., Lemoalle, J., Bricquet, J.P., 1996. Hydrologie du Lac Tchad (Lake Chad hydrology). Monographie hydrologique 12, ORSTOM (Office de la Recherche Scientifique et Technique d'Outre-Mer) éditions. p. 266.
Ouaidrari, H., Vermote, E.F., 1999. Operational atmospheric correction of Landsat TM data. Remote Sensing of Environment 70, 4–15.
Sakamoto, T., Nguyen, N.V., Kotera, A., Ohno, H., Ishitsuka, N., Yokozawa, M., 2007. Detecting temporal changes in the extent of annual flooding within the Cambodia and the Vietnamese Mekong Delta from MODIS time-series imagery. Remote Sensing of Environment 109, 295–313.
Scholte, P., 2005. Floodplain Rehabilitation and the Future of Conservation and Development: Adaptive Management of Success in Waza-Logone. Cameroon, Leiden University.
Smith, L., 1997. Satellite remote sensing of river inundation area, stage, and discharge: a review. Hydrological Processes 11, 1427–1439.
Storey, J., Scaramuzza, P., Schmidt, G., Barsi, J., 2005. Landsat 7 scan line corrector-off gap filled product development. In: Pecora 16 ''Global Priorities in Land Remote Sensing'' Proceedings. American Society for Photogrammetry and Remote Sensing. Sioux Falls, South Dakota.
Tou, J.T., Gonzales, R.C., 1974. Pattern Recognition Principles. Isodata Algorithm, Pattern Classification by Distance Functions. Addison-Wesley, Reading, Massachusetts. pp. 97–104.
Wesseling, J.W., Drijver, C.A., Nah E., Namba, A., Zuiderwijk, A., 1994. Waza Logone Flood Restoration Study: Identification of Options for Re-flooding. Leiden and Delft, the Netherlands: Center of Environmental Sciences, Leiden University and Delft Hydraulics.
Westra, T., De Wulf, R.R., 2009. Modelling yearly flooding extent of the Waza-Logone floodplain in northern Cameroon based on MODIS and rainfall data. International Journal of Remote Sensing 30, 5527–5548.
Westra, T., Mertens, K.C., De Wulf, R.R., 2005. ENVISAT ASAR wide swath and SPOT-VEGETATION image fusion for wetland mapping: evaluation of different wavelet-based methods. Geocarto International 20, 21–31.
Williams, D.L., Goward, S., Arvidson, T., 2006. Landsat: yesterday, today, and tomorrow. Photogrammetric Engineering and Remote Sensing 72, 1171–1178.